Biomaterials Science

PAPER

View Article Online
View Journal

Cite this: DOI: 10.1039/d5bm01898f

Enhanced corneal retention of hyaluronic acid *via* a metabolic glycoengineering-based *in vivo* bioorthogonal reaction

Buwei Hu,[a,b] Hui Wang,[f] Chenlin Ji,[b,e] Xuehan Xu,[b,e] Luyi Wang,[b,e] Tingting Cao,[b,e] Menghua Gao,[b,c,d] Yanjun Zhao,[g] Bin Wang,*[h] Wenjing Xuan*[b,c,d] and Jianjun Cheng *[b,c,d]

Received 27th December 2025,
Accepted 6th March 2026

DOI: 10.1039/d5bm01898f

rsc.li/biomaterials-science

Topical hyaluronic acid (HA) formulations have been extensively employed for managing various ocular diseases, but their therapeutic efficacy is severely compromised by rapid precorneal clearance due to a dense, negatively charged sialic acid-rich glycocalyx. To address this, we report a corneal surface engineering strategy that involves the metabolic incorporation of bioorthogonal azide groups onto the corneal epithelium. This covalent "docking" layer enables site-specific, Click chemistry-mediated immobilization of anionic HA, thereby significantly enhancing its ocular surface retention *in vitro* and *in vivo*. First, an alkyne-bearing molecule (DBCO) was labelled with a fluorescent probe (Cy5) to produce DBCO-Cy5. Sequential incubation of human corneal epithelial cells (HCECs) with an unnatural azide-bearing sugar (AAM) and DBCO-Cy5 enhanced the Cy5 retention by more than 10-fold. Then, HA was covalently labelled with DBCO at different conjugation ratios (HA-DBCO), and these conjugates showed negligible cytotoxicity. HA-DBCO binding to AAM-pretreated cells was time- and concentration-dependent; a higher degree of substitution substantially improved the reaction efficiency. Meanwhile, the covalent conjugation of HA to the cell surface did not affect HCEC proliferation but enhanced cell migration. The proof-of-concept was also validated in a mouse model of dry eye disease. AAM was ocularly delivered *via* a cationic liposome, resulting in the predominant deposition of azide in the corneal epithelium of mice. Subsequent dosing of HA-DBCO induced the *in vivo* bioorthogonal reaction that enhanced HA retention (up to 6 h) by 2.5-fold compared to the control without AAM pretreatment. The prolonged corneal retention enhanced the therapeutic efficacy at a reduced dosing frequency. This approach offers a clinically translatable strategy to improve the efficacy of topical HA-based therapies for ocular diseases.

Introduction

Hyaluronic acid (HA) is a biodegradable anionic glycosaminoglycan and an FDA-approved polymer widely used in ophthalmology to manage conditions, including dry eye disease (DED).[1] Due to its ability to retain water through hydrogen bonding, HA can stabilize the tear film and lubricate the ocular surface.[2] Beyond these physical mechanisms, HA exerts multifaceted biological activities by promoting corneal epithelial wound healing through enhanced cell migration, proliferation, suppressing inflammation, and mitigating free radical-induced damage.[3–5] HA is often administered as topical eye drops, which are non-invasive and patient-compliant.[6] However, its clinical efficacy is limited by the rapid tear turnover, the blink reflex, and the dense anionic glycocalyx of the corneal epithelium.[7–10] Together, these multi-tiered barriers result in a short precorneal residence, and the clinical utility of conventional HA eye drops is typically less than 30 minutes, necessitating a high drug concentration, increased HA molecular weight, and frequent dosing.[11] These approaches often lead to severe adverse effects, including elevated intraocular pressure, epithelial toxicity,[12–14] blurred vision and impeded normal blinking.[15–18]

[a]Department of Materials Science, Fudan University, Shanghai 200433, China
[b]Department of Materials Science and Engineering, Westlake University, Hangzhou, Zhejiang 310030, China. E-mail: chengjianjun@westlake.edu.cn
[c]Research Center for Industries of the Future, Westlake University, Hangzhou, Zhejiang 310030, China
[d]Institute of Advanced Technology, Westlake Institute for Advanced Study, Hangzhou, Zhejiang 310024, China
[e]School of Material Science and Engineering, Zhejiang University, Hangzhou, Zhejiang 310023, China
[f]School of Science, Westlake University, Hangzhou, Zhejiang 310030, China
[g]Tianjin Key Laboratory for Modern Drug Delivery & High Efficiency, School of Pharmaceutical Science & Technology, Faculty of Medicine, Tianjin University, Tianjin 300072, China
[h]Department of Ophthalmology, Tongde Hospital of Zhejiang Province, Hangzhou, Zhejiang 310012, China

Several strategies have been developed to overcome these limitations. However, each is constrained by inherent shortcomings. Methyl cellulose and hydroxypropyl methylcellulose are used as HA substitutes, but they also exhibit short ocular surface persistence and lack HA's inherent therapeutic benefits.[19] Therefore, there remains an unmet need for enhanced corneal retention of HA. Wang *et al.* reported an adhesive nanocoating of tannic acid and poly(2-methypropylene glycol phosphate choline), enabling the prolonged retention and sustained release of dexamethasone.[20] Lee *et al.* developed a polymer-peptide conjugate to enhance the ocular surface adhesion of an ocular therapeutic macromolecule.[21] These assemblies rely heavily on non-covalent interactions, which are weakened by shear stress and dilution, limiting their durability to minutes. Alternatively, cationic nanoparticles have been employed to improve ocular drug retention, and the mechanism of action involves electrostatic adhesion to the anionic ocular surface.[22] Such a method can increase drug uptake tenfold, but the long-term administration of a cationic carrier can lead to dose-dependent irritation and corneal epithelial sloughing.[7] Therefore, it is urgent to discover novel ocular delivery strategies featuring high corneal affinity and good biocompatibility.

Inspired by the corneal mucin glycocalyx, a structure densely decorated with negatively charged sialic acid, we hypothesized that metabolic glycoengineering could transform this natural repulsive barrier into a programmable anchoring platform. The bioorthogonal reaction, characterized by its high specificity and efficiency, has emerged as a biocompatible tool for biological and medical applications.[23–28] By supplying a tetraacetyl-*N*-azidoacetylmannosamine (Ac_4ManNAz) precursor in eye-drop form, we exploit this intrinsic machinery to install azide tags onto surface glycans. Following the establishment of this azide modification, dibenzocyclooctyne (DBCO)-functionalized HA was administered. This approach enables a copper-free, strain-promoted azide–alkyne cycloaddition (SPAAC) reaction to covalently conjugate HA to the azide modified corneal surface. Our *in vivo* studies confirm that this local Click reaction significantly enhances ocular surface retention, achieving a 2.5-fold increase in the HA signal. Moreover, the HA retention time is prolonged to at least 6 hours with this strategy. In DED treatment analysis, the Click-enhanced delivery system improves treatment efficacy compared with traditional administration routines. Furthermore, this strategy can reduce dosing frequency without influencing therapeutic outcomes in the DED mouse model. This innovative approach provides a novel strategy for developing ocular drug-delivery systems to prolong corneal residence time of therapeutic agents.

Results and discussion

HA-DBCO synthesis and characterization

Hyaluronic acid is a widely used ingredient in clinical artificial tear formulations. However, its hydrophilicity and anionic nature limit its retention on the negatively charged ocular surface, resulting in frequent administration in clinical application.[29,30] To address this limitation, we designed a metabolic glycoengineering strategy to enhance HA retention properties on the corneal surface. This approach involves the introduction of azide groups onto corneal surface sialic acids *via* the intrinsic metabolic pathway. Subsequently, dibenzocyclooctyne-decorated HA (denoted HA-DBCO) can specifically react with these azide groups through the Click reaction. This process can conjugate HA with the corneal surface, thereby improving HA retention. Crucially, to avoid affecting HA biofunctions, including water retention *via* hydrogen bonding through its hydroxyl groups and cell signalling *via* receptor interactions, we selectively conjugated the DBCO moiety to the carboxyl groups within the HA backbone.[31,32] This molecular design preserved the integrity of HA's essential hydration and cell signalling capabilities (Fig. 1a).

HA-DBCO molecules were synthesized *via* a two-step process.[33] First, the carboxyl group of HA was activated by using ethyldimethylaminopropyl carbodiimide/*N*-hydroxysuccinimide (EDC/NHS). Subsequently, amine-DBCO was introduced at predetermined ratios to produce HA derivatives with different degrees of substitution (DS). The products were characterized by ^{1}H nuclear magnetic resonance (^{1}H NMR). The results indicated that HA-DBCO showed a signal in the aromatic region (7.0–8.0 ppm) post modification, confirming the successful conjugation of DBCO to the HA backbone (Fig. S1). The degree of substitution of HA-DBCO was determined to be 1.9%, 4.0% and 12.5%, respectively. Since the

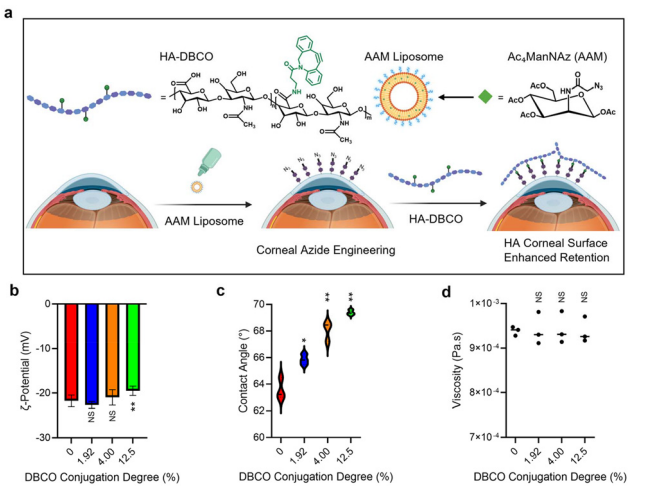

Fig. 1 Characterization of DBCO decorated hyaluronic acid. (a) Scheme of the corneal surface bioorthogonal reaction enhanced HA retention; (b) ζ-potential of HA with different DBCO conjugation degrees (1 mg mL^{-1}, n = 3); (c) contact angle illustration of HA with different DBCO conjugation degrees (1 mg mL^{-1}, n = 3); and (d) viscosity of HA with different degrees of DBCO decoration (1 mg mL^{-1}, n = 3). The statistical analysis was made with reference to the DBCO conjugation degree 0% group unless otherwise stated (*p < 0.05, **p < 0.01, NS, no significant difference; HA-DBCO, DBCO decorated HA; AAM, Ac_4ManNAz).

conjugation occurs at the anionic carboxylate group, we investigated its effect on the polymer's charge. The zeta-potential (ζ) measurements indicated that while the net negative charge of HA-DBCO slightly decreased with increasing DS, all derivatives maintained a strongly negative potential of approximately −20 mV (Fig. 1b). Furthermore, we assessed the potential impact of HA hydrophilicity after DBCO modification. Contact angle measurements confirmed a dose-dependent decrease in hydrophilicity with increasing DS (Fig. 1c and S2). In contrast, the viscosity of the HA-DBCO solutions at clinically relevant concentrations remained unaffected after modification (Fig. 1d). Collectively, these results demonstrate that DBCO functionalization subtly alters surface wettability and has a minimal impact on HA solution viscosity and surface charge.

Human corneal epithelial cell (HCEC) metabolic labelling analysis

The corneal epithelium expresses mucins that form the primary defensive barrier on the ocular surface. These mucins comprise heterogeneous glycoproteins, with glycocalyx structures being densely decorated with sialic acid residues.[34,35] The negatively charged mucin prevents the invasion of pathogens and manages the surface tension of the tear layer.[36,37] However, mucins also constitute the first barrier that the drug needs to overcome during ocular topical administration.[38] Building on the physiological evidence of high sialic acid expression on the corneal mucin glycocalyx, we hypothesized that metabolic glycoengineering could be used to introduce azide groups on the surface of corneal epithelial cells.

We first evaluated the efficiency of azide labelling on human corneal epithelial cells (HCECs) by supplementing the culture medium with $Ac_4ManNAz$ (AAM). The expression levels of azide-modified sialic acid were analysed *via* western blot and flow cytometry after different treatment durations (Fig. 2a). Our results demonstrated that HCECs could be effectively labelled with azide within 1 day of AAM treatment, and prolonging the treatment time did not significantly enhance labelling efficiency (Fig. 2b and c). Western blot analysis further confirmed that the azide tags were primarily incorporated into high molecular weight biomacromolecules and labelling achieved saturation after two days of treatment (Fig. 2d, e and S3). We then optimized the metabolic labelling conditions and found that corneal epithelial cells are susceptible to AAM. HCECs can achieve azide labelling saturation within 1 day, even at a low concentration of 3.12 μM (Fig. S4). Subsequent cytotoxicity assays demonstrated that AAM has appropriate biocompatibility for HCECs at the concentrations required for azide labelling (Fig. S5). Given that drug retention in topical ocular instillation is inherently limited, the high sensitivity of HCECs to AAM suggests that the corneal surface represents an ideal platform for efficient *in vivo* azide decoration.

For the cell surface Click reaction to proceed efficiently, the metabolically incorporated azide groups must be accessible on the cell membrane to facilitate contact with DBCO-functionalized molecules. To investigate the kinetics and subcellular localization of the bioorthogonal reaction, we treated azide labelled HCECs with a DBCO-conjugated Cy5 probe (DBCO-Cy5). HCECs were incubated with AAM for 2 days before proceeding with the DBCO-Cy5 treatment. Flow cytometry analysis revealed that the cell surface Click reaction was time-dependent, occurring within 1 minute after incubation with DBCO-Cy5. The azide modification of HCECs enhanced the attachment efficiency of DBCO-Cy5 by more than 10-fold compared with untreated control cells (Fig. S6). We next evaluated the retention time of the azide tags on the cell surface. HCECs pretreated with AAM were incubated in a standard culture medium for different days before assessing their reactivity with DBCO-Cy5 (Fig. 2f). The flow cytometry results demonstrated a gradual decrease in labelling intensity over time (Fig. 2g). Quantitative analysis of the mean fluorescence intensity (MFI) indicated that approximately 33% of the initial azide group on the cell surface remained after 3 days. Furthermore, HCECs still illustrated sufficient reactivity for enhanced DBCO-Cy5 attachment after 7 days of culture (Fig. 2h). Finally, confocal laser scanning microscopy (CLSM) was employed to visualize the subcellular location of the reaction. In contrast to untreated controls, AAM-pretreated cells exhibited robust DBCO-Cy5 fluorescence that colocalized with the cell membrane, confirming that bioorthogonal reaction occurs predominantly on the cell surface (Fig. 2i).

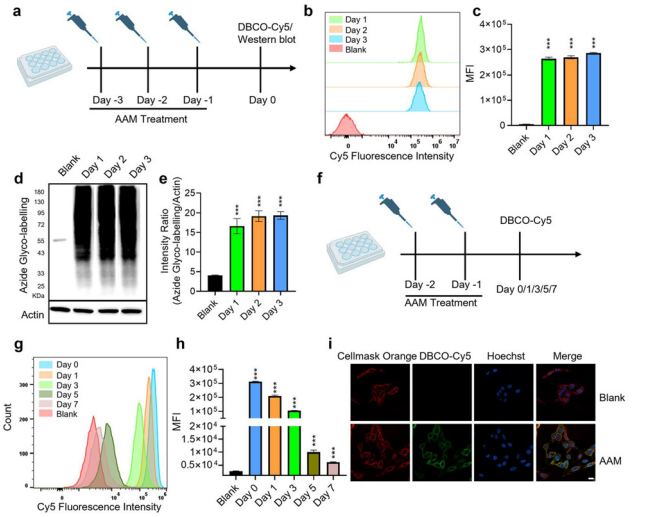

Fig. 2 HCEC cell surface azide labelling and Click reaction analysis. (a) Scheme of *in vitro* HCEC azide labelling efficiency analysis; (b) flow cytometry analysis of azide glycol labelling in the HCEC cell line for different AAM (50 μM) treatment days; (c) statistical analysis of flow cytometry results (n = 3); (d) western blot analysis of HCEC labelled with AAM (50 μM) for different treatment days; (e) statistical analysis of western blot results (n = 3); (f) scheme of *in vitro* HCEC azide retention analysis after treatment with AAM (50 μM) for two days; (g) flow cytometry analysis of azide retention on HCEC after AAM labelling; (h) statistical analysis of HCEC azide retention (n = 3); and (i) CLSM imaging of azide cellular distribution. Scale bar: 20 μm. The statistical analysis was performed with reference to the blank group unless otherwise stated (***p < 0.001; MFI, mean fluorescence intensity).

In vitro HA cell surface Click reaction analysis and biocompatibility analysis

After confirming the feasibility of the bioorthogonal reaction on HCEC surfaces using a small molecule probe, we next evaluated how DBCO functionalization influences the biological properties of HA. Given that HA biological functions and self-assembling secondary structure are regulated by interchain hydrogen bonding, we first assessed whether DBCO conjugation influences its biocompatibility.[39] The cytotoxicity assay revealed that DBCO decoration did not significantly affect HCEC viability until the DS reached 12.5% (Fig. S7). We then investigated the kinetics of the cell surface bioorthogonal reaction. Flow cytometry showed that HA-DBCO binding to azide-labelled cells was time-dependent, and higher DS substantially improved reaction efficiency (Fig. 3a). Quantitative analysis of the MFI indicated that HA-DBCO$_{12.5\%}$ exhibited the most rapid binding, achieving the highest signal enhancement within 5 minutes. However, consistent with the biocompatibility results, its efficiency declined after 15 minutes, possibly due to the onset of cytotoxicity. In contrast, HA-DBCO$_{4\%}$ demonstrated an optimal balance, combining appropriate biocompatibility with steadily increasing attachment, and achieving the highest reaction efficiency after 15 minutes of incubation (Fig. 3b). As a control, the absorption of unmodified HA (HA-DBCO$_{0\%}$) was also time- and concentration-dependent. However, it was not enhanced by AAM labelling (Fig. S8). On the basis of these cell surface Click reaction kinetics analysis results, HA-DBCO$_{4\%}$ was identified as the optimal conjugate and selected for all subsequent experiments.

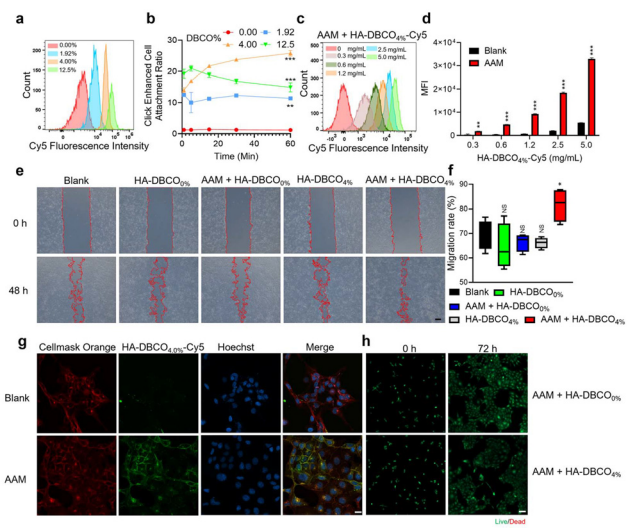

Fig. 3 HA-DBCO cell surface Click reaction kinetics, cell membrane targeting and biocompatibility analysis. (a) Flow cytometry analysis of the HCEC surface reaction of HA with different DBCO decoration degrees, HCEC pre-treated with AAM (50 μM) for two days; (b) statistical analysis of *in vitro* Click enhanced HA attachment (n = 3). The statistical analysis was performed with reference to the DBCO conjugation degree 0% group; (c) concentration-dependent cell surface Click reaction kinetics of HA-DBCO$_{4\%}$-Cy5; (d) statistical analysis of flow cytometry results of (c) (n = 3); (e) cell migration analysis of HCEC with or without AAM (50 μM) after two days of labelling and treatment with HA-DBCO$_{0\%}$ or HA-DBCO$_{4\%}$. Scale bar: 200 μm; (f) cell migration rate analysis (n = 4); (g) CLSM imaging of cellular distribution of HA-DBCO$_{4\%}$-Cy5 after the Click reaction. Scale bar: 20 μm; and (h) cell proliferation analysis of HCEC labelled with AAM (50 μM) for two days and treated with HA-DBCO$_{0\%}$ or HA-DBCO$_{4\%}$. Scale bar: 100 μm. The statistical analysis was performed with reference to the blank group under corresponding conditions unless otherwise stated (*p < 0.05, **p < 0.01, ***p < 0.001, NS, no significant difference, min, minutes, h, hours).

Given that topically administered drugs are rapidly diluted by tear fluid, it is critical to evaluate the concentration-dependent kinetics of the bioorthogonal reaction.[40] We therefore incubated AAM-pretreated and untreated HCECs with a series of HA-DBCO$_{4\%}$ solutions at different concentrations. Flow cytometric analysis revealed that the bioorthogonal reaction was concentration-dependent, significantly enhancing cellular association even at 0.3 mg mL^{-1}, resulting in a 6-fold increase compared to untreated cells (Fig. 3c and d). Notably, at the clinically relevant concentration of 1.2 mg mL^{-1}, the bioorthogonal reaction mediated by HA-DBCO$_{4\%}$ achieved a pronounced 12-fold enhancement in HA attachment compared to the control without Click chemistry (Fig. S9).[41] This result illustrates the significant advantage of our strategy under clinical application conditions. The slight decrease in efficiency observed at even higher concentrations may be attributed to DBCO-mediated hydrophobicity and potential intermolecular side reactions.[42,43] Beyond its role as a drug carrier, HA is a native extracellular matrix component that regulates epithelial cell migration and proliferation. We thus investigated whether DBCO modification and subsequent cell surface conjugation alter these biological functions. The cell scratch assays indicated that covalent conjugation of HA to the cell surface significantly facilitated HCEC cell migration (Fig. 3e and f). The live/dead staining confirmed that HA conjugated to the cell surface did not significantly impair HCEC proliferation (Fig. 3h), demonstrating the biocompatibility of this system for *in vivo* applications. Finally, we visualized the subcellular distribution of HA after the Click reaction by using confocal microscopy. CLSM imaging demonstrated that the bioorthogonal reaction facilitated even spreading of HA across the cell membrane. In contrast, without azide labelling, HA-DBCO$_{4\%}$ tended to form irregular clusters on the cell surface (Fig. 3g). Since HA is known to stabilize the tear film and modulate corneal surface tension in dry eye treatment, the uniform coating achieved *via* Click chemistry presents a potential mechanism for forming a stable, protective HA layer on the corneal surface.[44,45]

In vivo metabolic glycol labelling formulation screening

To establish a bioorthogonal reaction platform on the cornea, the metabolic precursor AAM must be efficiently delivered to corneal epithelial cells. To our knowledge, the ocular AAM delivery vehicle and the corneal surface glycoengineering method remain absent. Inspired by the physiological structure of the corneal mucin and prior work on topical solid lipid nanoparticles for small molecule delivery, we hypothesized that cationic liposomes could serve as an efficient vehicle for

AAM delivery to the corneal surface. To assess this hypothesis, we formulated AAM using three distinct carrier models: DOPC liposomes (neutral-charged nanoparticle model), a 10% DMSO/Tween 80 solution (organic solvent model), and DOTAP liposomes (cationic liposome model). The DOPC and DOTAP liposomes were prepared according to the established protocol. The drug loading efficiency (DLE) analysis confirmed that DOPC and DOTAP-AAM liposomes had a DLE of 33.2% and 29.2%, respectively. The cationic DOTAP liposomes demonstrated excellent stability, with no significant changes in particle size and ζ-potential over 20 days (Fig. S10a and b). Cryo-electron microscopy (Cryo-EM) further confirmed that the DOTAP liposomes had spherical morphology, with an average diameter of approximately 200 nm (Fig. S10c). Subsequent analysis of AAM release kinetics revealed that both formulations released the majority of their AAM payload within two hours (Fig. S10d). To evaluate AAM delivery efficiency *in vivo*, each formulation (10 mg mL^{-1}, AAM) was topically administered to the mouse eyes three times daily for three consecutive days. Corneal lysates were then analysed by western blot using a previously reported method.[46] The results demonstrated that the cationic DOTAP liposomes achieved the highest azide labelling intensity, resulting in a 1.8-fold increase over the DMSO formulation. In contrast, the DOPC liposomes failed to produce significant labelling, likely due to poor adhesion to the negatively charged corneal surface (Fig. 4a, d and S11). Consequently, the DOTAP liposome formulation was selected for all subsequent studies.

We next optimized the labelling protocol by treating mouse eyes with AAM-loaded DOTAP liposomes for varying durations. Mouse eyes were treated with AAM DOTAP liposomes three times daily for different days, then samples were collected for western blot analysis. Western blot analysis of corneal lysates confirmed that azide labelling was detectable after just one day of treatment and intensified with prolonged administration (Fig. 4b, e and S12). Given that chronic use of cationic carriers can cause ocular toxicity.[47] We sought to determine the *in vivo* retention profile of the azide label, prompted by our *in vitro* findings showing that azide tags persisted on HCECs for up to 7 days. Mice were treated with the AAM liposome regimen for two days, and corneal samples were collected at different time points after treatment. The analysis revealed that the azide signal persisted for up to 7 days, compared with blank controls (Fig. 4c, f and S13). This extended retention, consistent with our *in vitro* findings, suggests the potential for multiple drug administrations following a single labelling procedure. Finally, confocal microscopy was employed to determine the spatial localization of the azide tags. Imaging of ocular cryosections revealed that the azide label was predominantly localized to the corneal epithelium, corroborating our hypothesis that epithelial cell-surface sialic acids are effectively tagged *via* this metabolic pathway (Fig. 4g). Collectively, these findings establish an efficient and durable method for corneal surface bioorthogonal functionalization, significantly expanding the clinical potential of Click-chemistry-based ocular drug-delivery systems.

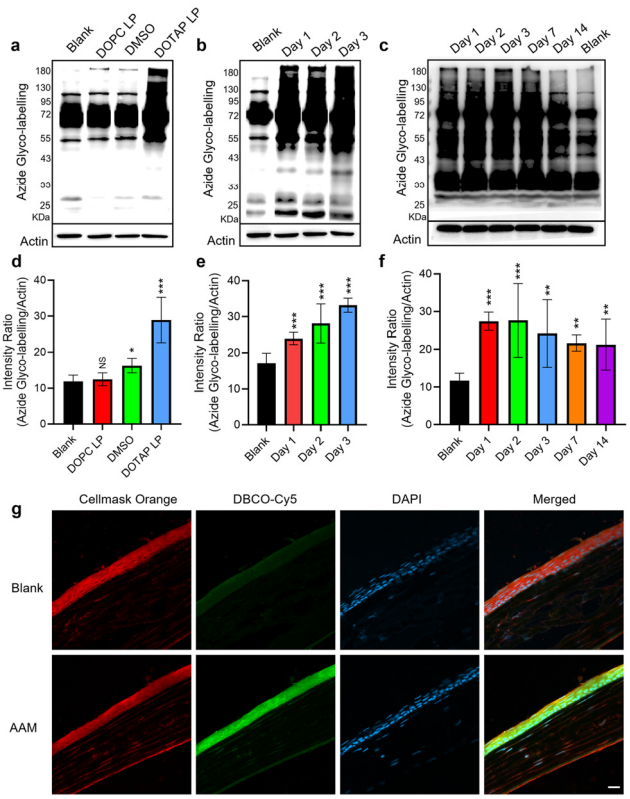

Fig. 4 *In vivo* ocular surface azide labelling method and its retention time analysis. (a) Western blot analysis of mouse eyes treated with different AAM (10 mg mL^{-1}) formulations; (b) western blot analysis of mouse eyes treated with AAM DOTAP liposome formulation (10 mg mL^{-1}) for different days; (c) western blot analysis of azide retention status for different days after AAM (10 mg mL^{-1}) topical administration for two days; (d) statistical analysis of western blot results of mouse eyes treated with different AAM formulations (n = 6); (e) statistical analysis of western blot results of mouse eyes treated with DOTAP formulation for different days (n = 6); (f) statistical analysis of western blot results of azide retention time for different days after AAM topical administration (n = 6); and (g) azide distribution in the ocular structure after DOTAP AAM liposome (10 mg mL^{-1}) labelling for two days, analysed by CLSM. Scale bar: 50 μm. The statistical analysis was performed with reference to the blank group unless otherwise stated (*p < 0.05, **p < 0.01, ***p < 0.001, NS, no significant difference, LP, liposome).

In vivo ocular surface Click-enhanced HA retention

Building on our findings that the cell surface Click reaction enhances HA retention *in vitro* and AAM-loaded DOTAP liposomes enable efficient corneal azide labelling, we hypothesized that this strategy could also significantly improve HA-DBCO attachment to the corneal surface *in vivo*. To test this, we topically applied $HA\text{-}DBCO_{4\%}$ or $HA\text{-}DBCO_{0\%}$ to mice with or without AAM liposome pretreatment (Fig. 5a). After 1 h, the mouse eyeballs were carefully collected for cryosection and fluorescence staining analysis. The mouse eyeball slides were analysed using a CLSM. While eyes treated with unmodified HA showed only weak fluorescence, those in the Click reaction group (AAM-pretreated + $HA\text{-}DBCO_{4\%}$) exhibited a strong fluorescent signal, forming a continuous HA layer on

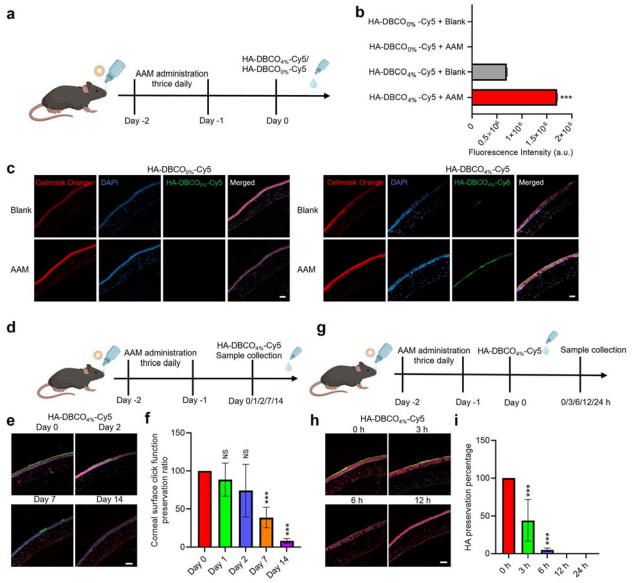

Fig. 5 *In vivo* ocular surface bioorthogonal reaction-based HA retention and its retention time analysis. (a) Scheme of *in vivo* corneal surface Click enhanced HA retention analysis; (b) semiquantitative analysis of Cy5 retained on the cornea in (c) obtained using ImageJ software (n = 6). The statistical analysis was made with reference to the HA-DBCO$_{4\%}$-Cy5 + Blank group; (c) CLSM image of HA-DBCO$_{0\%}$-Cy5 and HA-DBCO$_{4\%}$-Cy5 on the cornea with or without AAM (10 mg mL^{-1}) pretreatment for two days; (d) scheme of *in vivo* corneal surface azide functionality retention analysis and (e) CLSM image of HA-DBCO$_{4\%}$-Cy5 retained on cornea at different days after treatment with AAM liposome (10 mg mL^{-1}) for two days; (f) corneal surface Click function preservation status statistical analysis (n = 6). The statistical analysis was performed with reference to the Day 0 group; (g) scheme of *in vivo* corneal surface Click enhanced HA retention time analysis and (h) CLSM image of HA-DBCO$_{4\%}$-Cy5 retention time on cornea treated with AAM liposome (10 mg mL^{-1}) for two days; and (i) HA preservation status statistical analysis (n = 6). The statistical analysis was made with reference to the 0 h group. Scale bar: 50 μm (***p < 0.001, NS, no significant difference, h, hours).

the corneal surface (Fig. 5c). Semi-quantitative analysis confirmed that the bioorthogonal reaction enhanced HA attachment by approximately 2.5-fold compared to the control without AAM pretreatment (Fig. 5b). We then optimized the AAM liposome administration regimen based on Click-enhanced HA retention efficiency. Histological sections of mouse corneas and semi-quantitative analysis indicated that the bioorthogonal Click reaction began to significantly enhance HA attachment after two days of labelling (Fig. S14). Consequently, this two-day pretreatment protocol was adopted for all subsequent *in vivo* studies. Given our western blot data indicating azide persistence for at least 7 days, we next evaluated the durability of this enhancement *in vivo*. We applied HA-DBCO$_{4\%}$ at various time points after the initial azide labelling and assessed HA attachment *via* CLSM (Fig. 5d). The results demonstrated that a uniform HA coating could still be formed on the corneal surface as late as day 3 after labelling (Fig. 5e). Semi-quantitative analysis revealed that even on day 7, the azide tags retained about 40% of their initial functionality for enhancing HA attachment (Fig. 5f). This extended functional window significantly reduces the required frequency of AAM administration, thereby mitigating potential risks associated with repeated cationic carrier application. With these results, the corneal surface bioorthogonal reaction system demonstrated its potential for treating chronic eye disorders. Finally, we investigated the retention time of a single HA dose with Click reaction facilitation. After corneal azide labelling, a single dose of HA-DBCO$_{4\%}$ was administered, and eyeballs were collected at different time points for analysis (Fig. 5g). CLSM imaging showed that a distinct HA layer was maintained on the corneal surface for up to 3 hours, with a detectable signal still present at 6 hours (Fig. 5h and i). Further semi-quantification indicated that approximately 33% of the initial HA signal remained at the 3-hour mark. Since our previous data confirmed that azide tags persist on the cornea for over 24 hours, the observed decline in the HA signal is possibly attributed to the enzymatic degradation of HA by hyaluronidases present in the tear film, rather than the loss of the azide anchor.[48,49]

In vivo dry eye disease treatment efficacy and biocompatibility analysis

Based on the promising results demonstrating that the ocular surface Click reaction significantly enhances HA retention, we further explored its therapeutic potential in a DED mouse model. The DED model was established by topical application of 0.2% benzalkonium chloride (BAC) for four consecutive days. Mice in the Click-enhanced treatment group were pretreated with AAM liposomes (10 mg mL^{-1}) for two days, followed by topical administration of 0.4% HA-DBCO$_{0\%}$ or HA-DBCO$_{4\%}$ according to the schedule outlined in Fig. 6a. To assess corneal recovery, fluorescein sodium staining was performed and evaluated using a slit lamp. Given that the disease state may alter corneal metabolism, we first confirmed that azide labelling remained efficient in the DED model. Western blot analysis of DED corneal lysates after AAM liposome treatment confirmed successful azide incorporation (Fig. S15 and S16). With this validation, we proceeded to evaluate the therapeutic efficacy. Corneal epithelial defects were quantified using fluorescein staining scores. The results demonstrated that the Click-enhanced group (AAM + HA-DBCO$_{4\%}$) demonstrated advantages in corneal recovery compared to all other controls (Fig. 6b and c). Specifically, the Click-enhanced group exhibited a smoother corneal surface by day four, whereas the fluorescein signal remained visible in the other groups on day six (Fig. 6b). Furthermore, we challenged the system with a reduced dosing frequency. Remarkably, with corneal surface Click chemistry facilitation, administering HA-DBCO$_{4\%}$ once daily resulted in similar therapeutic outcomes to a twice-daily regimen (Fig. 6b and d). This indicates that the covalent anchoring strategy not only enhances treatment efficacy but also allows for a substantial reduction in dosing frequency. Subsequent immunofluorescence staining illustrated that the corneal surface Click reaction-enhanced treatment significantly reduced the levels of pro-inflammatory mediators (TNF-

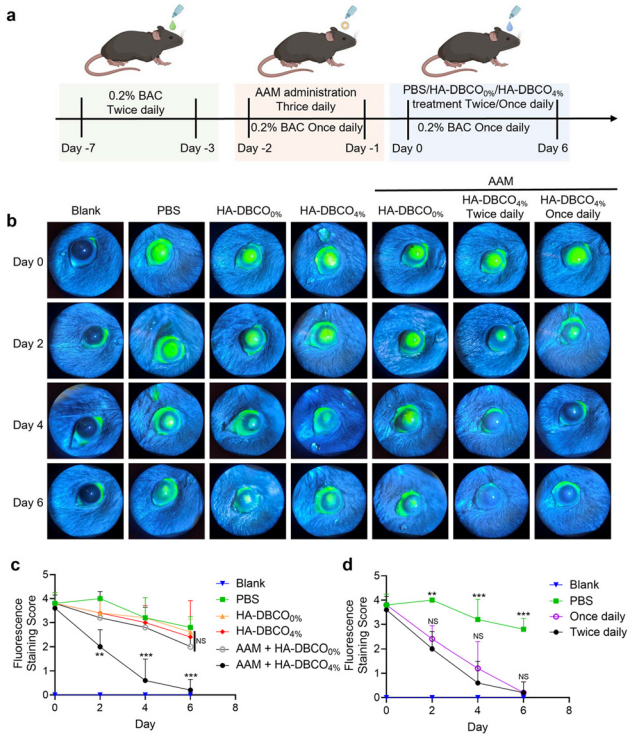

Fig. 6 Dry eye disease treatment efficacy analysis. (a) Schematic representation of the *in vivo* dry eye disease treatment regimen; (b) representative fluorescein sodium staining images (green color when photographed with a cobalt blue filter); the corresponding staining scores for the fluorescein sodium staining of (c) ocular surface Click reaction enhanced HA retention for dry eye disease treatment (n = 5). The statistical analysis was made with reference to the PBS group; and (d) treatment efficacy of different HA-DBCO$_{4\%}$ administration frequencies (n = 5), the statistical analysis was performed with reference to the twice daily group (**p < 0.01, ***p < 0.001, NS, no significant difference, BAC, benzalkonium chloride).

α, IL-1β) and the matrix-degrading enzyme MMP-9. In contrast, the treatments without the Click reaction enhancement (*i.e.*, HA-DBCO$_{4\%}$ and HA-DBCO$_{0\%}$) significantly diminished therapeutic effects (Fig. S17). This dataset illustrates that enhancing HA retention on the ocular surface can effectively reduce excessive reactive oxygen species (ROS), thereby relieving subsequent cellular damage and localized inflammation, which is crucial for effective DED therapy.[50,51] Consistent with this mechanism, the experimental group with only AAM-liposome treatment exhibited no therapeutic enhancement in the DED model (Fig. S18), illustrating the necessity of the HA-based retention strategy. Systemic biocompatibility assessments confirmed that the treatment did not adversely affect primary organ histology or body weight throughout the study (Fig. S19). Collectively, these findings substantiate the potential of the corneal surface Click chemistry platform as an effective and efficient strategy for treating dry eye disease.

This study demonstrates that covalent conjugation of HA to the corneal surface *via* a bioorthogonal Click reaction successfully resolves the challenges of rapid tear clearance and electrostatic repulsion in ocular drug delivery. Through metabolic glycoengineering, the negatively charged sialic acids are decorated with azide functional groups, enabling rapid and site-specific HA conjugation. This strategy facilitates the formation of a long-lasting HA coating that acts as a sustained-release reservoir, in contrast to the conventional eye drops with much shorter retention time. Despite these promising results, further investigation into several key aspects is necessary before clinical translation. First, the long-term biological effects of corneal azide modification and covalent HA conjugation on corneal epithelial cells still need further evaluation. Second, the potential immunogenicity associated with long-term polymer attachment to the corneal surface must be systematically analysed. Additionally, a more efficient and patient compliant method for introducing azide groups needs to be developed to facilitate clinical application. Addressing these inquiries will be essential for processing this ocular delivery technology toward clinical application.

Conclusion

In this study, we developed a novel metabolic glycoengineering strategy that repurposes the mucin sialic acid of the cornea. By employing metabolic glycoengineering, we introduced azide groups as chemical handles onto the corneal surface. This modification enabled the subsequent covalent conjugation of HA-DBCO *via* a bioorthogonal reaction. This approach resulted in the formation of a uniform HA layer on the cornea, which enhanced HA retention by 2.5-fold compared to conventional methods. Further evaluation in a DED model demonstrated that the Click-enhanced system resulted in a better corneal recovery status compared with the non-Click control. Interestingly, this strategy reduced HA dosing frequency without affecting final treatment performance. This *in situ*-formed HA matrix serves as a sustained-release depot for therapeutic agents. Furthermore, the uniform HA layer provides continuous physical protection and lubrication of the ocular surface. In summary, this study introduces an effective strategy for ocular drug delivery by utilizing the intrinsic physiological structure of the cornea for exogenous functionalization. This strategy illustrated potential for improving the efficacy and safety of topical treatments for a range of chronic ocular disorders.

Experimental

Materials and devices

Hyaluronic acid (HA, MW = 3 kDa) was purchased from OriLeaf Co., Ltd (Shanghai, China). Tetraacetyl-*N*-azidoacetylmannosamine (AAM) was purchased from Aladdin Co., Ltd (Shanghai, China). Dibenzocyclooctyne-amine (DBCO-NH$_2$) and 1-(2-carboxyethyl)-1,2,3,3-tetramethylindotricarbocyanine (Cy5-NH$_2$) were purchased from Jiangsu Aikang Biopharmaceutical Co., Ltd (Nanjing, China). 1,2-Dioleoyl-*sn*-

glycero-3-phosphocholine (DOPC), (2,3-dioleyl-propyl)-trimethylamine (DOTAP), and 1,2-distearoyl-*sn-glycero*-3-phosphoethanolamine-polyethylene glycol (DSPE-PEG2000) were purchased from AVT Pharmaceutical Tech Co., Ltd (Shanghai, China). All mentioned biological assay kits were obtained from Beyotime Biotechnology Co., Ltd (Shanghai, China). Hoechst 33342, DAPI, and CellMask Orange were obtained from Thermo Fisher Scientific Co., Ltd (USA). DBCO-Cy5, DBCO-Biotin, and Streptavidin-Horseradish Peroxidase (HRP) were obtained from Sigma-Aldrich Co., Ltd (USA). All other chemical reagents were obtained from Sinopharm Chemical Reagent Co., Ltd (Shanghai, China). All antibodies were obtained from Abcam Co., Ltd (Shanghai, China). All reagents were used as received without further purification or treatment.

Nuclear magnetic resonance (NMR) spectra were acquired on a Bruker Avance III 600 spectrometer using deuterated solvents. Zeta potential and particle size were assessed using a wide-angle dynamic light scattering/zeta potential analyzer (Brookhaven, USA). Ocular histology slides were prepared using a Cryostat CM1950 (Leica, Germany). Cellular toxicities were assessed using a Spectramax Max i5 microplate reader. Cellular fluorescence was analysed using a CytoFLEX (Becton Dickinson Caliper) and a confocal laser scanning microscope (CLSM, Carl Zeiss 980). Protein bands were visualized using a Bio-Rad ChemiDoc MP imaging system (Hercules, USA). HPLC analysis was performed by using an LC/MSD system (Agilent, 1260 Infinity II).

Preparation of HA-DBCO and characterization

HA (50 mg, 1 equiv., MW = 3 kDa) was dissolved in water at a concentration of 50 mg mL^{-1} and stirred overnight until fully dissolved. To functionalize HA with DBCO, EDC·HCl (142.5 mg, 0.746 mmol, 6 equiv.) and NHS (88.6 mg, 0.77 mmol, 6.2 equiv.) were dissolved in DMSO and added to the reaction solution sequentially. Then, various doses of DBCO-NH_2 (0.006 mmol, 0.024 mmol, 0.062 mmol) were dissolved in DMSO, added to the reaction, and the pH was adjusted with triethylamine (17.2 μL, 0.12 mmol). For Cy5-labelled HA-DBCO, Cy5-NH_2 (0.48 mg, 0.0006 mmol) was added to the reaction after pH adjustment. The reaction mixture was stirred at room temperature for 24 h. Afterwards, the product was dialyzed against DMF (6 × 0.5 L) for 2 days, followed by dialysis in water (6 × 2 L) for another 2 days, and then lyophilized. The final product was characterized by ^1H NMR.

Cell culture

Human corneal epithelial cells (HCECs) were obtained from Procell (Wuhan, China) and incubated in a standard cell culture medium consisting of DMEM supplemented with 10% heat-inactivated FBS (fetal bovine serum), penicillin (100 units per mL), streptomycin (100 μg mL^{-1}), and human epidermal growth factor (10 ng mL^{-1}). The cells were cultured in an incubator under a 5% CO_2 atmosphere at 37 °C. All cell culture consumables were obtained from Wisent Inc., Ltd (Canada).

AAM, HA, and HA-DBCO cytotoxicity analysis

For AAM cytotoxicity, cells were seeded at 5000 cells per well into 96-well plates and cultured overnight to allow attachment. The culture media were then removed and replaced with fresh media containing AAM at various concentrations (200, 100, 50, 25, 12.5, 6.25, 3.12, and 1.56 μM). After 24 hours of incubation, the cells were washed three times with PBS. Cell viability was assessed using the methyl thiazolyl tetrazolium (MTT) assay kit, according to the manufacturer's instructions.

For HA and HA-DBCO cytotoxicity analysis, cells were pretreated with or without AAM, then seeded at 5000 cells per well into 96-well plates and cultured overnight to allow attachment. The culture media were then removed and replaced with fresh media containing various concentrations of HA or HA-DBCO (10, 5, 2.5, 1.2, 0.6, and 0.3 mg mL^{-1}). After 1 hour of incubation, the cells were washed three times with PBS and further cultured overnight in standard culture media. Cell viability was analysed using the MTT assay according to the kit instructions.

In vitro metabolic glycoengineering and characterization

For concentration-dependent kinetics analysis of azide labelling, cells were seeded at 1×10^5 cells per well into 12-well plates and cultured overnight in standard cell culture medium. The cells were then washed with PBS, and the culture media were exchanged for media supplemented with AAM at various concentrations (100, 50, 25, 12.5, 6.25, and 3.12 μM), followed by incubation for 1 day. Afterward, the cells were washed three times with PBS and incubated with a DBCO-Cy5 (50 μM) solution for 1 h at 37 °C. Fluorescence signals from the cells were detected by flow cytometry.

For kinetic azide labelling western blot analysis, cells were seeded at 1×10^5 cells per well into 12-well plates and cultured overnight in standard cell culture medium. The cells were then washed with PBS, and the culture media were exchanged for media supplemented with AAM (50 μM), and the cells were incubated for different durations. Azide-labelled cells were analysed by western blot following a previously reported procedure.[46] Briefly, azido-modified biomacromolecules in cell lysates were biotinylated by incubation with DBCO-biotin. Streptavidin-HRP and an enhanced chemiluminescence (ECL) kit were then used to detect the HRP signal on the membrane with a ChemiDoc Imaging System. For flow cytometry analysis, cells were washed three times with PBS and incubated with a DBCO-Cy5 (50 μM) solution for 1 h at 37 °C. Fluorescence signals from the cells were detected by flow cytometry.

For azide cell retention analysis, cells were pretreated with AAM (50 μM) for 2 days, then seeded at 3×10^4 cells per well into 12-well plates and cultured overnight in standard cell culture medium. The cells were then further cultured in standard cell culture medium for different durations. Finally, the cells were washed three times with PBS and incubated with a DBCO-Cy5 solution (50 μM) for 1 h at 37 °C. Fluorescence signals from the cells were detected by flow cytometry.

In vitro HA-DBCO and DBCO-Cy5 cell surface Click reaction analysis

To investigate the cell-surface Click reaction kinetics, HCECs pretreated with or without AAM were seeded at 1×10^5 cells per well in 12-well plates and cultured overnight. The cells were then washed three times with PBS and incubated with HA-DBCO-Cy5 or HA-Cy5 solutions at different concentrations (5, 2.5, 1.2, 0.6, and 0.3 mg mL^{-1}) for 30 min. Finally, the cells were washed three times with PBS, collected, and analysed by flow cytometry.

To investigate the Click reaction kinetics, a procedure similar to the concentration-dependent study was followed. Cells were incubated with HA-DBCO-Cy5 or HA-Cy5 (1 mg mL^{-1}) at 37 °C for different durations (1, 5, 15, 30, and 60 min). After incubation, the cells were collected and analysed by flow cytometry.

For DBCO-Cy5 cell-surface Click reaction kinetics, HCECs pretreated with or without AAM were seeded at 1×10^5 cells per well in 12-well plates and cultured overnight. The cells were then incubated with DBCO-Cy5 (10 μM) at 37 °C for different durations (1, 5, 15, 30, and 60 min). After incubation, the cells were collected and analysed by flow cytometry.

Cell scratch and live & dead staining analysis

For the cell scratch assay, HCECs were seeded at 3×10^5 cells per well in 12-well plates and cultured overnight with or without AAM pretreatment. The medium of the monolayer was then replaced with medium containing 1% FBS and incubated for 4 h. Subsequently, wounds of approximately 500 μm in size were created by mechanically scratching the monolayer with a sterile 100 μL pipette tip. Detached cells and debris were removed by washing with PBS. The scratched monolayer was then incubated with 0.1% HA or HA-$DBCO_{4\%}$ for 1 h under standard cell culture conditions. Afterward, cells were washed with PBS and incubated with serum-free cell culture medium for different time intervals (0, 12, 24, and 48 h). Wound closure was monitored using an inverted phase contrast microscope (Zeiss, Germany).

For the cell proliferation assay, HCECs were seeded at 3×10^4 cells per well in 12-well plates and cultured overnight with or without AAM pretreatment. The cells were then incubated with HA or HA-$DBCO_{4\%}$ for 1 h under standard cell culture conditions; this treatment was repeated every 24 hours. After each PBS wash, the cells were cultured in standard cell culture medium for different time intervals (0, 24, 48, and 72 h). Cell proliferation status was analysed using live/dead staining and imaged with a fluorescence microscope.

HA-DBCO and cell membrane targeting and azide subcellular distribution analysis

For HA-DBCO cell membrane targeting analysis, HCECs with or without AAM pre-treatment were seeded at 5×10^4 cells per dish in confocal dishes. After overnight incubation, the cells were washed three times with PBS and subsequently treated with HA-DBCO-Cy5 (1 mg mL^{-1}) for 1 h at 37 °C. The cells were then stained with CellMask Orange (1 μg mL^{-1}) for 15 min at room temperature to label the cell membrane and with Hoechst (2 μg mL^{-1}) for 10 min at 37 °C to label nuclei. All images were acquired using a confocal laser scanning microscope (CLSM).

For azide subcellular distribution analysis, HCECs with or without AAM pre-treatment were seeded at 5×10^4 cells per dish in confocal dishes. After overnight incubation, the cells were washed three times with PBS and subsequently treated with DBCO-Cy5 (50 μM) for 1 h at 37 °C. The cells were then stained with CellMask Orange (1 μg mL^{-1}) for 15 min at room temperature to label the cell membrane and with Hoechst (2 μg mL^{-1}) for 10 min at 37 °C to label nuclei. All images were acquired using a CLSM.

AAM liposome and DMSO formulation preparation

The DOPC anionic AAM liposome was prepared following a previously described protocol.[52] The DOTAP cationic AAM liposome was prepared based on the DOPC formulation, using a lipid composition of DOPC/DOTAP/Cholesterol/DSPE-PEG2000 at a molar ratio of 10/40/50/2. The lipid components were dissolved in dichloromethane (DCM), and AAM was dissolved in DCM and mixed with the lipid solution. The mixture was then rotary evaporated to remove DCM. Subsequently, PBS was added to the flask to achieve an AAM concentration of 10 mg mL^{-1}, and the mixture was ultrasonicated for 1.5 h on ice. The final product was filtered through a 0.22 μm filter to generate uniform AAM liposomes. The DMSO formulation was prepared by dissolving AAM (25 mg) in a DMSO/Tween 80/PBS (10/15/75, v/v/v) solution. Specifically, AAM was first dissolved in DMSO (250 μL), then mixed with Tween 80 (375 μL), and finally diluted with PBS (1875 μL) to obtain a transparent AAM solution for topical administration.

The encapsulation efficiency and release behaviour were analysed following previous research.[53] Briefly, following preparation, the liposomes were purified *via* size-exclusion chromatography using a Sephadex G-25 column with PBS as the eluent to remove unencapsulated small molecules. To determine the DLE, the liposome solution (5.0 mg mL^{-1}) was diluted 10-fold with an acetonitrile (ACN)–water solution (1 : 1, v/v) to disrupt the vesicles. The amount of encapsulated AAM was then quantified by HPLC against an AAM standard curve. The release profile was assessed by dispersing the AAM-loaded liposomes in PBS to a final concentration of 50 μM. Subsequently, 800 μL of this dispersion was loaded into a dialysis bag (MWCO: 3.5 kDa), which was immersed in 19.2 mL of PBS as the release medium and incubated at 37 °C with gentle shaking (50 rpm). At predetermined time intervals (0, 0.1, 0.2, 0.4, 0.6, 1, 2, 4, 8, and 12 h), 0.4 mL of the external medium was collected. Each sample was reacted with 2 μM DBCO-Cy5 in ACN for 24 h at 37 °C. The remaining DBCO-Cy5 was quantified by HPLC, and the concentration of released AAM was calculated using a reverse-titration method.

Mouse maintenance

Mouse experiments were conducted with the approval of the Animal Care and Use Committee of Westlake University. The

mice were sourced from GemPharmatech Co., Ltd (Jiangsu, China) and raised under standard conditions. All animal experiments were conducted following the guidelines for the care and use of laboratory animals. The experimental protocols were reviewed and approved by the Institutional Animal Care and Use Committee (IACUC) at the School of Engineering, Westlake University (AP#21-051). Female C57/B6 mice (17–22 g) were used for *in vivo* metabolic glycoengineering, HA retention, and dry eye disease treatment research.

In vivo ocular metabolic glycoengineering and characterization

For analysis of AAM delivery formulation screening, AAM DOPC liposomes, DOTAP liposomes, and the DMSO formulation solution (10 mg mL^{-1}) were topically administered to the right eyes of mice (n = 6, 5 μL per administration) thrice daily for three consecutive days. Afterwards, the mouse eyeballs were collected and processed for western blot analysis following the previously described protocol.

For analysis of cationic AAM liposome labelling time screening, the AAM DOTAP cationic liposome (10 mg mL^{-1}) was topically administered to the right eyes of mice (n = 6, 5 μL per administration) for different days. Afterwards, the mouse eyeballs were collected and processed for western blot analysis following the previously described protocol. For cryosection analysis, the DOTAP cationic liposome (10 mg mL^{-1}) was topically administered to the right eyes of mice (n = 3, 5 μL per administration) for three consecutive days. Subsequently, the mouse eyeballs were collected, embedded in the OCT compound, and sectioned into 10 μm-thick cryosections for fluorescence staining analysis.

For ocular azide labelling retention analysis, the DOTAP cationic liposome (10 mg mL^{-1}) was topically administered to the right eyes of mice (n = 6, 5 μL per administration) for two consecutive days. The mouse eyeballs were then collected at different time points (0, 1, 2, 7, and 14 days) after the final AAM liposome administration. The collected eyeballs were processed for western blot analysis following the previously described protocol.

In vivo HA corneal surface Click reaction enhanced attachment and retention analysis

For analysis of Click reaction-enhanced HA attachment, a DOTAP cationic liposome (10 mg mL^{-1}) was topically administered to the right eyes of mice (n = 6, 5 μL per administration) for 2 days. The left eyes served as the blank control without AAM treatment. HA-Cy5 and HA-$DBCO_{4\%}$-Cy5 were dissolved in PBS at 0.4%. HA-Cy5 or HA-$DBCO_{4\%}$-Cy5 was then topically administered to the mouse eyes (5 μL per eye). The mouse eyeballs were collected 1 hour post-administration, embedded in OCT medium, and processed for cryosectioning and subsequent fluorescence staining.

For the analysis of HA corneal retention time, a DOTAP cationic liposome (10 mg mL^{-1}) was topically administered to the right eyes of mice (n = 6 and 5 μL per administration) for 2 days. The left eye served as the blank control without AAM treatment. HA-$DBCO_{4\%}$-Cy5 was dissolved in PBS to 0.4% and administered topically at 5 μL per eye. One hour after administration, the eyes were rinsed with PBS. The mouse eyeballs were collected at different time points (0, 3, 6, 12, and 24 h) after HA-$DBCO_{4\%}$ treatment, embedded in OCT medium, and processed for cryosectioning.

For fluorescence staining, the eyeball sections were equilibrated to room temperature for 15 min and then rehydrated in PBS for 15 min. The slides were blocked with 5% BSA in PBS for 1 h at room temperature. For immunofluorescence staining, the IL-1β, TNF-α, and MMP-9 antibodies were diluted in a 1 : 300 (v/v) ratio and incubated with slides at 4 °C overnight. Then, Alexa 647 secondary antibody (1 : 500, v/v) was incubated with slides for 1 h at room temperature. Subsequently, the slides were stained with CellMask Orange (1 μg mL^{-1}) for 15 min at room temperature to label cell membranes and with DAPI (2 μg mL^{-1}) for 10 min at room temperature to label nuclei. Finally, the slides were mounted with an anti-fade mounting medium and stored at 4 °C before imaging. All images were acquired using a CLSM system.

In vivo corneal surface azide function retention time analysis

DOTAP cationic liposome (10 mg mL^{-1}) was topically administered to the right eyes of mice (n = 6), 5 μL per administration, for 2 days. HA-$DBCO_{4\%}$-Cy5 was dissolved in PBS at 0.4%. HA-$DBCO_{4\%}$-Cy5 was then topically administered to the mouse eyes at different time intervals (0, 1, 2, 7, and 14 days) after AAM labelling, with 5 μL administered to each eye. The mouse eyeballs were collected, embedded in OCT medium, and cryosectioned to generate slides for fluorescence staining analysis. Fluorescence staining was performed according to the previously described protocol.

In vivo dry eye disease treatment analysis

The DED mouse model was established by topical administration of 0.2% benzalkonium chloride (BAC). A volume of 5 μL was applied to the right eye of each mouse (n = 5 per group) for four consecutive days. Subsequently, regarding the mice in the azide-labelled groups, 5 μL of DOTAP AAM liposome was topically administered to the right eye for two consecutive days. The remaining control groups received an equivalent volume of PBS instead. Following this pretreatment, the therapeutic agents—PBS (vehicle control), 0.4% HA-$DBCO_{0\%}$, or HA-$DBCO_{4\%}$—were applied to the right eye of the mice. Each agent was administered at a volume of 5 μL per dose, with a frequency of twice daily or once daily, as specified in the experimental design. Throughout the entire treatment period, a 0.2% BAC solution was applied once daily to all mice to sustain the DED state. To evaluate corneal epithelial recovery, fluorescein sodium staining was performed. Briefly, a 0.5% fluorescein sodium solution was applied, and the resulting fluorescence signal was observed and documented using a slit lamp equipped with a cobalt blue filter.

Statistical analysis

Statistical analyses were conducted using GraphPad Prism version 10.3.0. To compare the two groups, we utilized the

unpaired, two-tailed Student's *t*-test with a 95% confidence interval. *$p < 0.05$, **$p < 0.01$ and ***$p < 0.001$ were considered statistically significant.

Author contributions

Buwei Hu: conceptualization, methodology, formal analysis, investigation, data curation, and writing – review & editing. Hui Wang: chemical synthesis support. Chenlin Ji: chemical synthesis support. Bin Wang: conceptualization, methodology, animal experiment technical support, and equipment provider. Yanjun Zhao and Wenjing Xuan: writing – review & editing. Jianjun Cheng: project administration, resources, supervision, funding acquisition, and writing – review & editing. The manuscript was written through contributions of all authors. All authors have approved the final version of the manuscript.

Conflicts of interest

There are no conflicts to declare.

Data availability

Data will be made available on request. The data supporting the findings of this study have been included as part of the supplementary information (SI). Supplementary information is available. See DOI: https://doi.org/10.1039/d5bm01898f.

Acknowledgements

This work was supported by the "Pioneer" and "Leading Goose" R&D Program of Zhejiang (2024SDXHDX0004) and the National Natural Science Foundation of China (52233015 for J. C., 22407112 for M. G. and 22407111 for W. X.). J. C. acknowledges support from the New Cornerstone Investigator Program, New Cornerstone Science Foundation (NCI202332).

References

1 M. J. Rah, *Optometry*, 2011, **82**, 38–43.
2 M. E. Johnson, P. J. Murphy and M. Boulton, *Graefes Arch., Clin. Exp. Ophthalmol.*, 2006, **244**, 109–112.
3 J. Andrade del Olmo, V. Sáez Martínez, N. Martínez de Cestafe, J. M. Alonso, C. Olavarrieta, M. Ucelay López de Heredia, S. Benito Cid and R. Pérez González, *Carbohydr. Polym. Technol. Appl.*, 2024, **8**, 100577.
4 L. Hynnekleiv, M. Magno, E. Moschowits, K. A. Tønseth, J. Vehof and T. P. Utheim, *Acta Ophthalmol.*, 2024, **102**, 25–37.
5 G. Carracedo, C. Pastrana, M. Serramito and C. Rodriguez-Pomar, *Acta Ophthalmol.*, 2019, **97**, e162–e169.
6 F. A. Maulvi, K. H. Shetty, D. T. Desai, D. O. Shah and M. D. P. Willcox, *Int. J. Pharm.*, 2021, **608**, 121105.
7 C. Wang and Y. Pang, *Adv. Drug Delivery Rev.*, 2023, **194**, 114721.
8 A. Y. Yang, J. Chow and J. Liu, *Yale J. Biol. Med.*, 2018, **91**, 13–21.
9 I. Brockhausen, E. Elimova, A. M. Woodward and P. Argüeso, *Carbohydr. Res.*, 2018, **470**, 50–56.
10 T. Jia, F. Stapleton, F. Iqbal, J. Showyin, D. Roy, M. Roy and J. Tan, *Optom. Vis. Sci.*, 2024, **101**, 603–607.
11 Y. Yang and A. Lockwood, *Exp. Eye Res.*, 2022, **218**, 109006.
12 L. Quaranta, A. Novella, M. Tettamanti, L. Pasina, R. N. Weinreb and A. Nobili, *Ophthalmol. Ther.*, 2023, **12**, 2227–2240.
13 C. Baudouin, A. Labbé, H. Liang, A. Pauly and F. Brignole-Baudouin, *Prog. Retinal Eye Res.*, 2010, **29**, 312–334.
14 R. E. Ruiz-Lozano, N. S. Azar, H. M. Mousa, M. E. Quiroga-Garza, S. Komai, L. Wheelock-Gutierrez, C. Cartes and V. L. Perez, *Front. Toxicol.*, 2023, **5**, 1067942.
15 M. Ali and M. E. Byrne, *Pharm. Res.*, 2009, **26**, 714–726.
16 E. B. Papas, D. Tilia, D. Tomlinson, J. Williams, E. Chan, J. Chan and B. Golebiowski, *Optom. Vis. Sci.*, 2014, **91**, 24–31.
17 X. Zhang, D. Wei, Y. Xu and Q. Zhu, *Carbohydr. Polym.*, 2021, **264**, 118006.
18 M. Guter and M. Breunig, *Eur. J. Pharm. Biopharm.*, 2017, **113**, 34–49.
19 E. B. Papas, J. B. Ciolino, D. Jacobs, W. L. Miller, H. Pult, A. Sahin, S. Srinivasan, J. Tauber, J. S. Wolffsohn and J. D. Nelson, *Invest. Ophthalmol. Visual Sci.*, 2013, **54**, 183–203.
20 C. Wang, X. Liu, W. Lv, X. Kuang, F. Wu, X. Fan and Y. Pang, *Sci. Adv.*, 2025, **11**, 18.
21 D. Lee, Q. Lu, S. D. Sommerfeld, A. Chan, N. G. Menon, T. A. Schmidt, J. H. Elisseeff and A. Singh, *Acta Biomater.*, 2017, **55**, 163–171.
22 B. Jurišić Dukovski, M. Juretić, D. Bračko, D. Randjelović, S. Savić, M. Crespo Moral, Y. Diebold, J. Filipović-Grčić, I. Pepić and J. Lovrić, *Int. J. Pharm.*, 2020, **576**, 118979.
23 Y. Bo, J. Zhou, K. Cai, Y. Wang, Y. Feng, W. Li, Y. Jiang, S. H. Kuo, J. Roy, C. Anorma, S. H. Gardner, L. M. Luu, G. W. Lau, Y. Bao, J. Chan, H. Wang and J. Cheng, *Proc. Natl. Acad. Sci.*, 2023, **120**, e2302342120.
24 S. Lee, H. I. Yoon, J. H. Na, S. Jeon, S. Lim, H. Koo, S. S. Han, S. W. Kang, S. J. Park, S. H. Moon, J. H. Park, Y. W. Cho, B. S. Kim, S. K. Kim, T. Lee, D. Kim, S. Lee, M. G. Pomper, I. C. Kwon and K. Kim, *Biomaterials*, 2017, **139**, 12–29.
25 S. Lim, H. Y. Yoon, S. J. Park, S. Song, M. K. Shim, S. Yang, S. W. Kang, D. K. Lim, B. S. Kim, S. H. Moon and K. Kim, *Biomaterials*, 2021, **266**, 120472.
26 S. W. Kang, S. Lee, J. H. Na, H. I. Yoon, D. E. Lee, H. Koo, Y. W. Cho, S. H. Kim, S. Y. Jeong, I. C. Kwon, K. Choi and K. Kim, *Theranostics*, 2014, **4**, 420–431.
27 S. S. Han, H. E. Shim, S. J. Park, B. C. Kim, D. E. Lee, H. M. Chung, S. H. Moon and S. W. Kang, *Sci. Rep.*, 2018, **8**, 13212.

28 S. S. Han, D. E. Lee, H. E. Shim, S. Lee, T. Jung, J. H. Oh, H. A. Lee, S. H. Moon, J. Jeon, S. Yoon, K. Kim and S. W. Kang, *Theranostics*, 2017, **7**, 1164–1176.
29 I. Hargittai and M. Hargittai, *Struct. Chem.*, 2008, **19**, 697–717.
30 B. Grassiri, Y. Zambito and A. Bernkop-Schnürch, *Adv. Colloid Interface Sci.*, 2021, **288**, 102342.
31 W. Tian, B. Lin, X. Yang, H. Zhang, L. Li, L. Nie, X. Guo, S. Huang and H. Zang, *Asian J. Complementary Altern. Med.*, 2021, **9**, 28–31.
32 A. G. Tavianatou, I. Caon, M. Franchi, Z. Piperigkou, D. Galesso and N. K. Karamanos, *FEBS J.*, 2019, **286**, 2883–2908.
33 S. S. Han, H. Y. Yoon, J. Y. Yhee, M. O. Cho, H. E. Shim, J. E. Jeong, D. E. Lee, K. Kim, H. Guim, J. H. Lee, K. M. Huh and S. W. Kang, *Polym. Chem.*, 2018, **9**, 20–27.
34 I. K. Gipson, *Invest. Ophthalmol. Visual Sci.*, 2007, **48**, 4390–4391.
35 A. M. Woodward and P. Argüeso, *Invest. Ophthalmol. Visual Sci.*, 2014, **55**, 6132.
36 B. Yañez-Soto, M. J. Mannis, I. R. Schwab, J. Y. Li, B. C. Leonard, N. L. Abbott and C. J. Murphy, *Ocul. Surf.*, 2014, **12**, 178–201.
37 P. Argüeso, A. M. Woodward and D. B. AbuSamra, *Front. Immunol.*, 2021, **12**, 2021.
38 H. Han, Q. Yin, X. Tang, X. Yu, Q. Gao, Y. Tang, A. Grzybowski, K. Yao, J. Ji and X. Shentu, *J. Mater. Chem. B*, 2020, **8**, 5143–5154.
39 K. Palenčárová, R. Köszagová and J. Nahálka, *Int. J. Mol. Sci.*, 2025, **26**, 7028.
40 H. B. Mohamed, B. N. Abd El-Hamid, D. Fathalla and E. A. Fouad, *Eur. J. Pharm. Sci.*, 2022, **175**, 106206.
41 M. Moshirfar, K. Pierson, K. Hanamaikai, L. Santiago-Caban, V. Muthappan and S. F. Passi, *Clin. Ophthalmol.*, 2014, **8**, 1419–1433.
42 C. Zhang, P. Dai, A. A. Vinogradov, Z. P. Gates and B. L. Pentelute, *Angew. Chem., Int. Ed.*, 2018, **57**, 6459–6463.
43 S. H. Wong, S. N. Kopf, V. Caroprese, Y. Zosso, D. Morzy and M. M. C. Bastings, *Nano Lett.*, 2024, **24**, 11210–11216.
44 X. Zhang, M. Vimalin Jeyalatha, Y. Qu, X. He, S. Ou, J. Bu, C. Jia, J. Wang, H. Wu, Z. Liu and W. Li, *Int. J. Mol. Sci.*, 2017, **18**, 1398.
45 P. A. Knepper, S. Covici, J. R. Fadel, C. S. Mayanil and R. Ritch, *J. Glaucoma*, 1995, **4**, 194–199.
46 B. Hu, C. Ji, Z. Zhou, X. Xu, L. Wang, T. Cao, J. Cheng and R. Sun, *Biomater. Sci.*, 2025, **13**, 1233–1242.
47 J. Alvarez-Trabado, Y. Diebold and A. Sanchez, *Int. J. Pharm.*, 2017, **532**, 204–217.
48 M. Akkurt Arslan, F. Brignole-Baudouin, S. Chardonnet, C. Pionneau, F. Blond, C. Baudouin and K. Kessal, *Sci. Rep.*, 2023, **13**, 15231.
49 A. Ogunleye, A. Bhat, V. U. Irorere, D. Hill, C. Williams and I. Radecka, *Microbiology*, 2015, **161**, 1–17.
50 T. Zhou, S. Li, J. Zhu, G. Zeng, Z. Lv, M. Zhang, K. Yao and H. Han, *J. Controlled Release*, 2024, **373**, 306–318.
51 J. Bu, Y. Liu, R. Zhang, S. Lin, J. Zhuang, L. Sun, L. Zhang, H. He, R. Zong, Y. Wu and W. Li, *Antioxidants*, 2024, **13**, 422.
52 R. Xie, S. Hong, L. Feng, J. Rong and X. Chen, *J. Am. Chem. Soc.*, 2012, **134**, 9914.
53 L. Shen, K. Cai, J. Yu and J. Cheng, *Bioconjugate Chem.*, 2019, **30**, 2317–2322.

